Title No. 121-S43

Modeling of Glass Fiber-Reinforced Polymer-Reinforced Squat Walls under Lateral Loading

by Ju-Hyung Kim, Yail J. Kim, and Hong-Gun Park

This paper presents mechanics-based modeling approaches to understand the shear behavior of squat walls reinforced with glass fiber-reinforced polymer (GFRP) bars when subjected to lateral loading. The applicability of design provisions in published specifications is examined using collated laboratory test data, resulting in the need for developing revised guidelines. Analytical studies are undertaken to evaluate the effects of reinforcement type on the response of load-bearing walls and to establish failure criteria as a function of various stress states in constituents. Obvious distinctions are noticed in the behavior of squat walls with steel and GFRP reinforcing bars owing to their different reinforcing schemes, tension-stiffening mechanisms, and material properties. Newly proposed equations outperform existing ones in terms of predicting the shear capacity of GFRP-reinforced squat walls. Furthermore, based on geometric and reinforcing attributes, a novel determinant index is derived for the classification of structural walls into squat and slender categories, which overcomes the limitations of prevalent methodologies based solely on aspect ratio. A practical method is suggested to adjust the failure mode of walls with GFRP reinforcing bars, incorporating a characteristic reinforcement ratio.

Keywords: failure mode; glass fiber-reinforced polymer (GFRP); modeling; shear; squat wall.

INTRODUCTION

Shear walls are indispensable for a building structure to accommodate lateral loads. Improper designs accelerate the deterioration of load-bearing members and bring about serviceability problems such as excessive sidesway.[1] Placing shear walls in the right locations ensures the stability of building frames,[2] and the large wall stiffness controls the horizontal displacement of constituents within an acceptable limit stipulated in specifications.[3] When subjected to lateral loading, both ends of a wall (typically called boundary elements with concentrated reinforcing bars) carry tension and compression forces.[4] These elements, which are essential if the maximum compression stress near the end of a wall exceeds a certain limit,[5] are instrumental in resisting load reversals and inhibiting unanticipated buckling.[6] Depending upon aspect ratio (h_w/l_w, where h_w and l_w are the height and length of a wall, respectively), shear walls are categorized as squat and slender; however, no absolute demarcation is available from a behavioral perspective: a ratio between h_w/l_w = 1.0 and 2.0 often plays a role as a bifurcation point.[7-9] Among other particulars, the shear strength coefficient (α_c) of structural walls in ACI 318-19[5] may fulfill the demand for practical guidance (α_c = 3.0 for $h_w/l_w \leq 1.5$, 2.0 for $h_w/l_w \geq 2.0$, and a linearly interpolated value for $1.5 < h_w/l_w < 2.0$ in U.S. customary units). These classifications can be interpreted in a way that an aspect ratio is reasonably taken to be below 1.5 for squat walls and a ratio between 1.5 and 2.0 indicates a transition from squat to slender walls.

The application of non-metallic reinforcement has become commonplace around the globe[10]; accordingly, a building code with glass fiber-reinforced polymer (GFRP) reinforcing bars (ACI CODE-440.11-22[11]) was recently published to direct practicing engineers. While high strength, light weight, nonmagnetic composition, and low maintenance are some of the many advantages that GFRP composites offer, corrosion resistance is the most notable benefit when incorporated in concrete structures.[12] On the use of GFRP reinforcement for shear walls, a consensus has not yet been made. Some researchers argue that technical evidence is insufficient for field application[13]; by contrast, others claim that the non-yielding nature of GFRP with a low elastic modulus improves the seismic performance of concrete members.[14,15] As far as GFRP-reinforced squat walls are concerned, limited research has been reported and only a few experimental papers are available.[8,16] Further studies are thus necessary to understand the behavior of squat walls with GFRP reinforcing bars and to expand the applicable boundary of these nontraditional construction materials.

This paper discusses an analytical model to examine the response of GFRP-reinforced squat walls under lateral loading. With the aim of overcoming the limitations of technical findings from test data,[8,16] detailed mechanics are accounted for and design recommendations are elaborated. In addition, an alternative expression is suggested to identify a behavioral threshold between squat and slender walls, which is not simply reliant on an aspect ratio.

RESEARCH SIGNIFICANCE

The design of shear walls is empirical and heavily relies on practitioners' experience without systematic derivations.[17,18] Notwithstanding the broad adoption of GFRP reinforcement in concrete members, little is known about its use in squat walls. Because the failure mechanism of squat walls differs from that of slender walls (that is, the former tends to fail in shear, accompanied by diagonal tension cracks,

ACI Structural Journal, V. 121, No. 3, May 2024.
MS No. S-2023-172.R1, doi: 10.14359/51740489, received November 22, 2023, and reviewed under Institute publication policies.

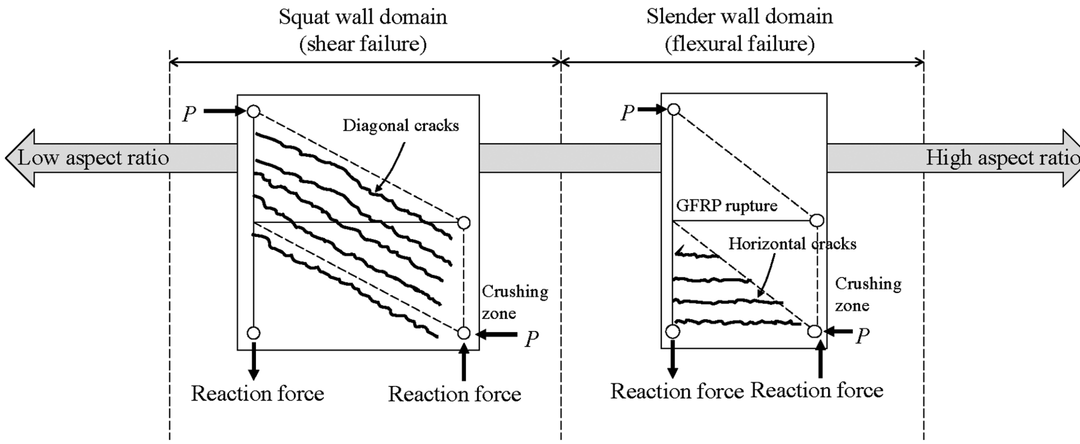

Fig. 1—Conceptual failure modes of GFRP-reinforced concrete walls.

whereas the latter fails in flexure[1]), archetypal methods that are predicated upon ductile responses cannot be applied. Furthermore, in view of deficient ductility in squat walls, attention should be paid to how premature shear failure can be precluded by employing adequate technical approaches. A refined mechanics-based model is developed to elucidate the intrinsic behavior of squat walls with GFRP reinforcing bars, leading to the proposal of practical design equations.

BACKGROUND

Expository discussions are presented with regard to the shear behavior of GFRP-reinforced concrete walls. Codified design provisions are reviewed and evaluated using test data, including a comparative analysis that investigates functional differences between squat walls with steel and GFRP reinforcing bars.

Potential failure modes

As conceptually visualized in Fig. 1, a GFRP-reinforced concrete wall may fail in flexure, shear, or a combination thereof. For instructional purposes, the load path of the wall is approximated with idealized joints connecting compression and tension segments (dotted and solid lines in Fig. 1, respectively). When the wall's aspect ratio is lower than a certain limit, its failure is governed by compression struts parallel to diagonal tension cracks in the web and by the crushing of the end zone (the squat wall domain in Fig. 1). If an aspect ratio is higher than the limit, the wall tends to bend like a cantilever fixed at the base and horizontal cracks formed within the tension zone; eventually, it fails by either the rupture of GFRP or the crushing of the concrete (the slender wall domain in Fig. 1). Contingent upon the properties of wall structures, a transition between these two scenarios can be seen.

Design method

Because the design of squat walls with GFRP reinforcement has not been fully documented in published specifications, the coalescence of ACI 440.1R-15,[12] ACI 318-19,[5] and ACI 440.11-22[11] may be used. The nominal shear capacity of a wall (V_n) is expressed as[5,11]

$$V_n = V_c + V_f \leq V_{n,max} \tag{1}$$

$$V_{n,max} = k_1 f_c'^{0.5} d t_w = k_2 f_c'^{0.5} l_w t_w \tag{2}$$

where V_c and V_f are the nominal shear resistance of the concrete and reinforcement, respectively; k_1 and k_2 are empirical constants (k_1 = 10 and k_2 = 8 for U.S. customary units and k_1 = 0.83 and k_2 = 0.66 for metric units[5]); t_w and l_w are the thickness and length of the wall, respectively; and d is the effective depth ($d = 0.8l_w$).[11] The individual components of Eq. (1) are provided by[11,12]

$$V_c = k_3 f_c'^{0.5} t_w k d = k_4 f_c'^{0.5} k l_w t_w \tag{3}$$

$$k = \sqrt{2\rho_f n_f + (\rho_f n_f)^2} - \rho_f n_f \tag{4}$$

$$V_f = A_{fv} f_{fv} d/s = \rho_h f_{fv} l_w t_w \tag{5}$$

$$f_{fv} = \Omega E_f \leq f_{fb} \tag{6}$$

where k_3 and k_4 are empirical constants (k_3 = 5 and 0.4 and k_4 = 4 and 0.32 for U.S. customary and metric units, respectively[11]); ρ_f is the reinforcement ratio ($\rho_f = A_{fv}/(bd)$, in which A_{fv} is the cross-sectional area of the shear reinforcement and b is the width of the wall); n_f is the modular ratio ($n_f = E_f/E_c$, in which E_f and E_c are the elastic moduli of the GFRP and concrete, respectively); s is the center-to-center spacing of the reinforcing bars; f_{fb} is the design strength of the bent stirrup made of GFRP; and Ω is the strain limit of the reinforcement (Ω = 0.004).[12]

Appraisal

Existing test data—Figure 2(a) shows a ratio between the experimental and nominal shear capacities of GFRP-reinforced squat walls (V_{test} and V_n, respectively). The properties of test specimens excerpted from Table 1 are as follows[8]: aspect ratio (h_w/l_w) = 0.68 and 1.14, compressive strength of concrete (f_c') = 33 to 40 MPa (4790 to 5800 psi), tensile strength of GFRP (f_{fu}; f_{uh} and f_{uv} for horizontal and vertical reinforcing bars in Table 1, respectively) = 1022 to 1100 MPa (148 to 160 ksi), and horizontal and vertical reinforcement ratios (ρ_h and ρ_v, respectively) = 0.38% to 0.7%. The specimens with h_w/l_w = 1.33 in Table 1 were excluded due to a low reinforcement ratio in the boundary element (ρ_{be} =

Table 1—Summary of existing test programs on GFRP-reinforced squat walls

No.	Reference	Specimen	h_w, mm	l_w, mm	h_w/l_w	t_w, mm	l_{be}, mm	f_c', MPa	f_{uh}, MPa	f_{uv}, MPa	f_{ul}, MPa	f_{ut}, MPa	ρ_h, %	ρ_v, %	ρ_{be}, %	ρ_t, %	$N/(A_g f_c')$, %	V_{test}, kN	Drift*, %	Failure mode
1	Arafa et al.[19]	G4-250	2000	1500	1.33	200	200	35	1372	1372	1020	1065	0.51	0.59	1.43	0.89	0	678	2.65	Flexure
2	Arafa et al.[19]	G4-160	2000	1500	1.33	200	200	35	1372	1372	1020	1065	0.79	0.59	1.43	0.89	0	708	2.80	Flexure
3	Arafa et al.[19]	G4-80	2000	1500	1.33	200	200	40	1372	1372	1020	1065	1.58	0.59	1.43	0.89	0	912	2.75	Flexure
4	Arafa et al.[19]	G6-80	2000	1500	1.33	200	200	41	1372	1372	1020	1065	3.56	0.59	1.43	0.89	0	935	2.90	Flexure
5	Arafa et al.[20]	G4	2000	1500	1.33	200	200	40	1372	1372	1020	1065	1.58	0.59	1.43	0.89	0	740	2.60	Flexure
6	Shabana et al.[8]	MSQ1	1600	1400	1.14	150	225	40	1100	1100	1100	1022	0.38	0.5	4.48	5.0	7.5	561	1.13	Shear
7	Shabana et al.[8]	MSQ2	1600	1400	1.14	150	225	39	1022	1100	1100	1022	0.38	0.5	4.48	5.0	15.0	590	1.17	Shear
8	Shabana et al.[8]	MSQ3	1600	1400	1.14	150	225	37	1022	1100	1100	1022	0.63	0.5	4.48	5.0	7.5	683	1.54	Shear
9	Shabana et al.[8]	MSQ4	1600	1400	1.14	150	225	37	1022	1100	1100	1022	0.63	0.7	4.48	5.0	7.5	732	1.81	Shear
10	Shabana et al.[8]	SSQ1	950	1400	0.68	150	225	35	1022	1100	1100	1022	0.38	0.5	4.48	5.0	7.5	1071	1.00	Shear
11	Shabana et al.[8]	SSQ3	950	1400	0.68	150	225	33	1022	1100	1100	1022	0.63	0.5	4.48	5.0	7.5	1102	1.10	Shear

*Lateral drift at failure.

Note: h_w is wall height; l_w is wall length; t_w is wall thickness; b_{be} is boundary element width; f_c' is concrete compressive strength; f_{uh} is tensile strength of web horizontal GFRP reinforcing bar; f_{uv} is tensile strength of web vertical GFRP bar; $f_{u,be}$ is tensile strength of GFRP reinforcing bar in boundary elements; ρ_h is web horizontal reinforcement ratio; ρ_v is web vertical reinforcement ratio; ρ_{be} is vertical reinforcement ratio in boundary elements; $N/(A_g f_c')$ is axial load ratio applied to top of wall; V_{test} is experimental capacity. 1 mm = 0.0394 in.; 1 MPa = 145 psi.

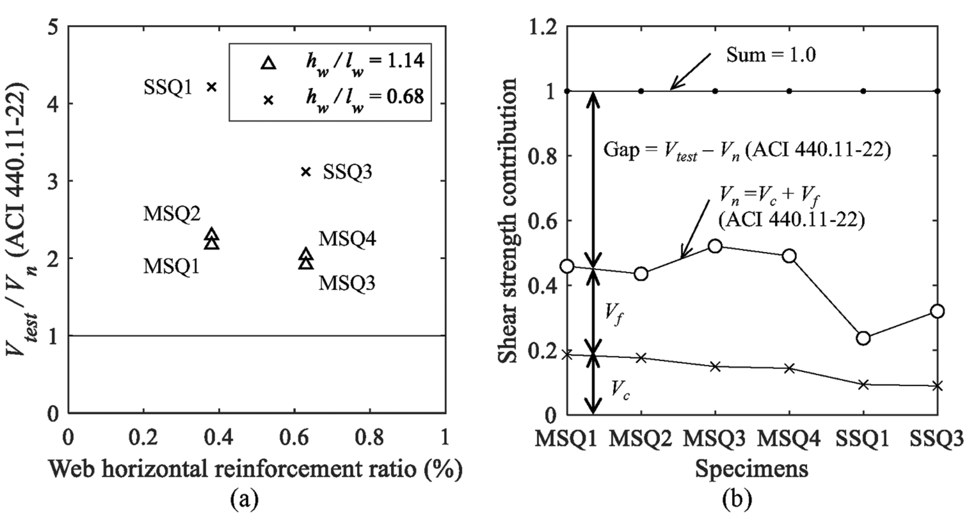

Fig. 2—ACI design approach for GFRP-reinforced concrete walls with an aspect ratio of less than 1.5: (a) shear capacity; and (b) contribution of components.

1.43%), which will be accounted for in a subsequent section. Although the number of test specimens in Fig. 2(a) is insufficient to render conclusive information, owing to a lack of available data, it is substantiated that Eq. (1) underestimated the capacity of the walls; especially, significant conservatism was noticed ($V_{test}/V_n > 3.0$) when the aspect ratio was $h_w/l_w = 0.68$. These discrepancies are ascribed to the fact that the expression of V_c in Eq. (1) was empirically calibrated using flexure-shear-combined responses alongside large diagonal tension cracks[12]; on the contrary, the shear-dominated behavior of the squat walls with a low aspect ratio entailed narrow inclined cracks parallel to the compression struts (Fig. 1). Accordingly, an improvement is required to better predict the capacity of squat walls with GFRP reinforcing bars, which can avert the placement of unnecessary shear reinforcement.

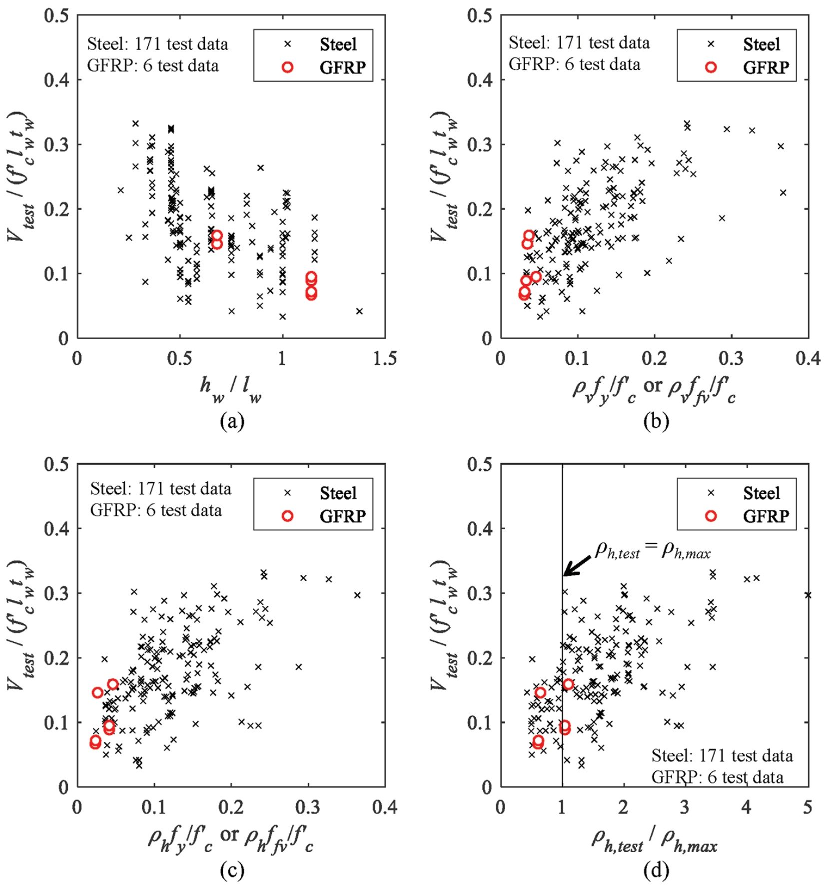

Fig. 3—Comparison of steel- and GFRP-reinforced squat walls: (a) aspect ratio; (b) normalized horizontal reinforcement ratio in web; (c) normalized vertical reinforcement ratio in web; and (d) ratio between horizontal reinforcement ratio and maximum reinforcement ratio.

The portion of the concrete and GFRP resistance (Eq. (3) and (5), respectively) is allocated in Fig. 2(b). For consistency, the allowable strain limit of $\Omega = 0.004$ was employed to calculate V_f in all specimens. The gap between the test and prediction spanned from 0.48 to 0.76 and the degree of margin ($V_{test} - V_n$) was apparent when the aspect ratio dropped to $h_w/l_w = 0.68$ (the SSQ series). This tendency again confirms that the design approach of ACI CODE-440.11-22[11] does not cover GFRP-reinforced concrete squat walls.

Comparison against steel reinforcement—To figure out behavioral differences between GFRP and steel reinforcing bars in squat walls, a comparative assessment was made. For steel-reinforced walls, a total of 171 test data were collated from literature[21-51] with the succeeding properties (those of GFRP-reinforced walls were delineated in the preceding section): h_w/l_w = 0.21 to 1.5; f_c' = 20 to 70 MPa (2900 to 10,150 psi); ρ_h and ρ_v = 0.25% to 2.8%; and f_y = 284 to 750 MPa (41 to 109 ksi), in which f_y is the yield strength of the reinforcing bars. Figure 3 graphs the test capacities of the walls, which were normalized by the cross-sectional area and concrete strength ($f_c' l_w t_w$) to accommodate variable geometric and material properties, as a function of primary design parameters. While the normalized capacities of both steel and GFRP cases decreased with an increase in the aspect ratio (Fig. 3(a)), their response range differed in the ordinate: $0.03 \leq V_{test}/(f_c' l_w t_w) \leq 0.33$ for steel and $0.07 \leq V_{test}/(f_c' l_w t_w) \leq 0.16$ for GFRP. Analogous patterns were noted for the normalized horizontal reinforcement ratios ($\rho_h f_y/f_c'$ for steel and $\rho_h f_{fv}/f_c'$ for GFRP) and vertical reinforcement ratios ($\rho_v f_y/f_c'$ for steel and $\rho_v f_{fv}/f_c'$ for GFRP) given in Fig. 3(b) and (c), respectively. These distinct ranges of wall capacities, depending upon the reinforcement type, can be explained by deriving the maximum horizontal reinforcement ratio ($\rho_{h,max}$) when the shear capacity of the walls ($V_{n\text{-}wall}$) is equivalent to their shear-strength limit ($V_{n,max}$, Eq. (2)), which represents the most critical state in a squat wall system: diagonal tension failure equals web-crushing.

The $V_{n\text{-}wall}$ expressions for the steel- and GFRP-reinforced concrete walls are attained from ACI 318 (Eq. (7))[5] and ACI CODE-440.11-22 (Eq. (1))[11]

$$V_{n\text{-}wall} = (\alpha_c \lambda f_c'^{0.5} + \rho_h f_{yh}) l_w t_w \tag{7}$$

where α_c is the shear strength coefficient (α_c = 3.0 and 0.25 for U.S. customary and metric units, respectively, for an aspect ratio of $h_w/l_w \leq 1.5$); and λ is the concrete strength factor (λ = 1.0 for ordinary concrete). After setting Eq. (7) = Eq. (2) and Eq. (1) = Eq. (2) for steel and GFRP-reinforced concrete walls, respectively, the horizontal reinforcement ratio (ρ_h) is solved, which is equivalent to the maximum reinforcement ratio of each instance ($\rho_{h,max}$)

$$\rho_{h,max} = \psi_1 \frac{f_c'^{0.5}}{f_{yh}} \text{ for steel reinforcement} \tag{8}$$

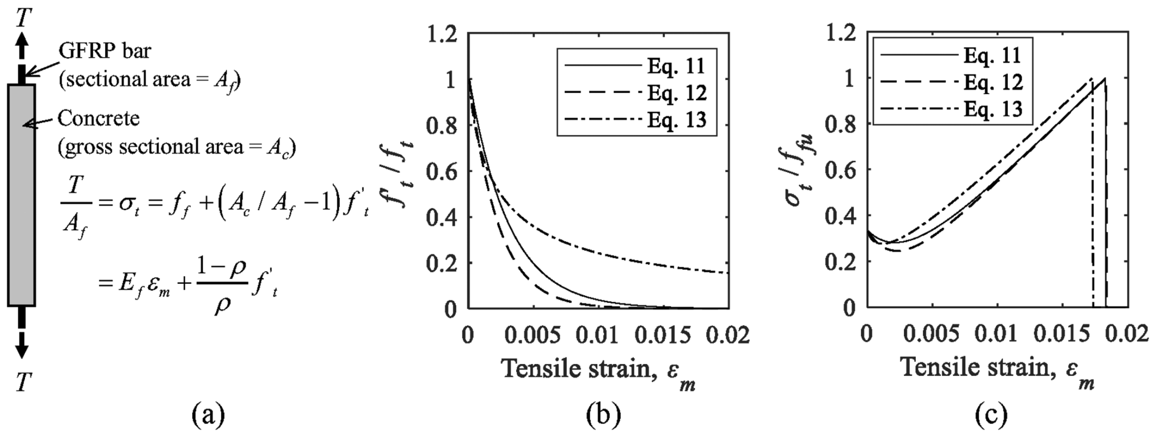

Fig. 4—Tension stiffening of GFRP-reinforced concrete: (a) schematic representation; (b) progressive reduction of tensile stress in concrete; and (c) strain-dependent response.

$$\rho_{h,max} = (\psi_2 - \psi_3 k)\frac{f_c'^{0.5}}{f_{fv}} \text{ for GFRP reinforcement} \quad (9)$$

where ψ_1, ψ_2, and ψ_3 are constants ($\psi_1 = 5$, $\psi_2 = 8$, and $\psi_3 = 4$ for U.S. customary units and $\psi_1 = 0.41$, $\psi_2 = 0.66$, and $\psi_3 = 0.34$ for metric units). As demonstrated in Fig. 3(d), the majority of reinforcement ratios in the steel-reinforced walls (136 specimens or 80% of the entire samples) exceeded the maximum ratio ($\rho_{h,max}$); contrarily, most ratios of walls with GFRP were close to or less than the maximum ratio. These observations clarify that the amount of reinforcing bars was generally greater in the steel-reinforced walls than their GFRP counterparts, which was related to the high strength of GFRP, and that the contribution of these reinforcing bars to the shear capacity of the walls was dissimilar, justifying the need for an independent design approach pertaining to GFRP-reinforced squat walls.

MODELING

To comprehend the ramifications of steel and GFRP reinforcing bars for the shear behavior of reinforced concrete squat walls, a twofold analytical model is formulated at the element and structural levels. This section outlines an overview of modeling processes along with implementation steps and verification against test data.

Element level

Framework—A unit square panel[52] represented shear-loaded wall elements with steel and GFRP reinforcing bars. The panel concrete had a tensile strength of f_t = 1.8 MPa (260 psi), resulting from f_c' = 30 MPa (4350 psi),[53] and was orthogonally reinforced with reinforcing bars at a reinforcement ratio of ρ = 0.25% to 3.0%. The lower bound of the ratio conformed to the requirement of ACI 318-19,[5] while the upper bound enveloped the ratios of the experimental specimens presented in Fig. 3. The yield and ultimate strengths of the steel and GFRP reinforcing bars were f_y = 420 MPa (60 ksi) and f_{fu} = 1100 MPa (160 ksi) with elastic moduli of E_s = 200 GPa (29,000 ksi) and E_f = 60 GPa (8700 ksi), respectively. The stress-strain behavior of the panel was computed as per the procedure of the Modified Compression Field Theory,[53] incorporating tension-stiffening that realistically considered interactions between the concrete and reinforcing bars.

Tension stiffening—A schematic representation of the tension-stiffening mechanism is shown in Fig. 4(a). The tensile stress of the reinforced concrete segment (σ_t) is calculated by the summation of reinforcing bar stresses inside the concrete (f_f) and the surrounding concrete (($A_c/A_f - 1)f_t'$, in which A_c and A_f are the cross-sectional areas of the concrete and reinforcing bar, respectively, and f_t' is the stress of the concrete with tensioning-stiffening)

$$\sigma_t = E_f\varepsilon_m + \frac{1-\rho}{\rho}f_t' \quad (10)$$

where ε_m is the tensile strain of the reinforced concrete. For the representation of tension stiffening in GFRP-reinforced concrete, three candidate expressions were chosen[54-56]

$$f_t' = f_t \exp\left[-1100(\varepsilon_m - \varepsilon_{cr})\left(\frac{E_f}{200{,}000}\right)\right] \quad (11)$$

$$f_t' = f_t \exp\left[-1500(\varepsilon_m - \varepsilon_{cr})\left(\frac{E_f}{200{,}000}\right)\right] \quad (12)$$

$$f_t' = f_t/\left(1 + \beta_1(\varepsilon_m - \varepsilon_{cr})\left[\left(\frac{E_f}{200{,}000}\right)\right]^{\gamma}\right) \quad (13)$$

where ε_{cr} is the concrete strain at cracking; and β_1 and γ are the tension-stiffening constants (β_1 = 1400 and γ = 0.8, 1.0, and 1.5 for ribbed, sand-coated, and helically wrapped GFRP bars, respectively[56]). As plotted in Fig. 4(b) and (c), the downward propensity of Eq. (11) and (12) was alike, whereas Eq. (13) overestimated the tension-stiffening effect. Given the marginal tension stiffening of GFRP-reinforced concrete members,[57] Eq. (12) was used in this study. For the occasion of steel-reinforced concrete, the tension-stiffening model of Vecchio and Collins[53] was adopted

$$f_t' = f_t/(1 + (200\varepsilon_m)^{0.5}) \quad (14)$$

Constitutive relationship—Figures 5(a) and (b) reveal the stress-strain relationship of the steel-and GFRP-reinforced

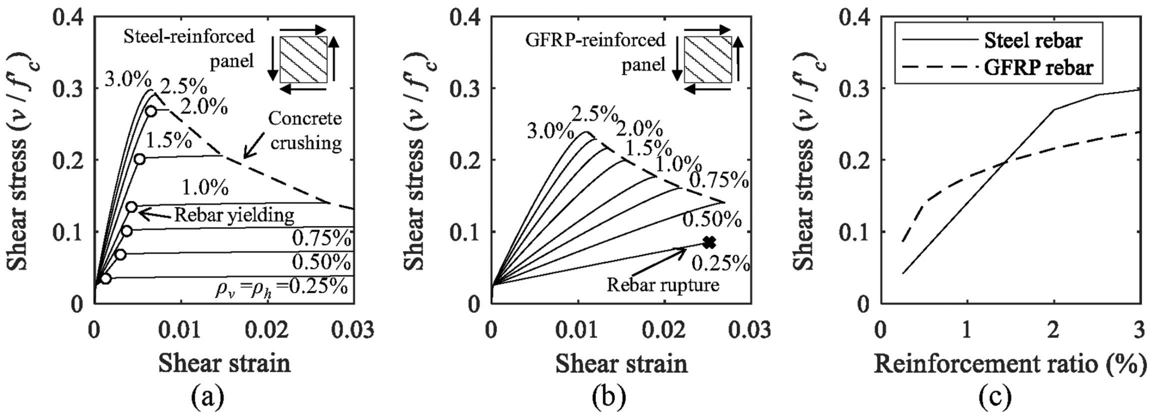

Fig. 5—Element-level shear behavior: (a) steel-reinforced concrete panel; (b) GFRP-reinforced concrete panel; and (c) comparison of maximum shear stresses.

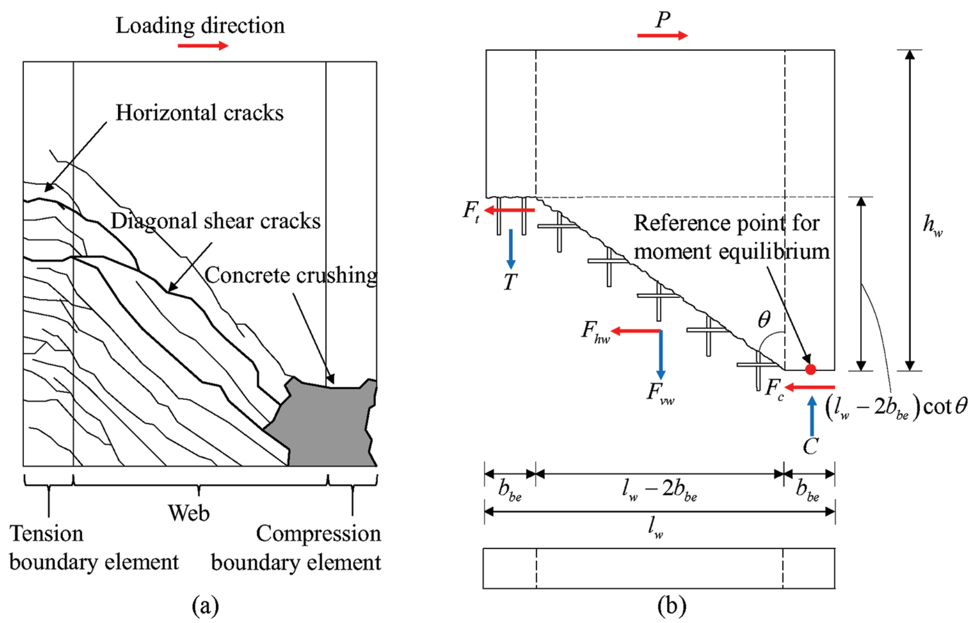

Fig. 6—Analytical model: (a) test observation; and (b) simplified free body diagram.

concrete panels loaded in shear, respectively. To focus on the disparity of these reinforcing bar types, the average stress values (v) in the ordinate were normalized by the concrete strength (f_c'). The failure of the steel-reinforced panel was attributed to the yielding of the reinforcing bars combined with the crushing of the concrete (Fig. 5(a)), except for the heavily reinforced panel having $\rho \geq 2.5\%$ that failed without yielding. On the GFRP-reinforced panel (Fig. 5(b)), concrete crushing was responsible for the failure, with the exception of the lightly reinforced panel ($\rho = 0.25\%$). The low elastic modulus of GFRP caused much increase in strain under the same stress level, compared with the steel-reinforced case. Shown in Fig. 5(c) is a compilation of the maximum shear stresses with the reinforcement ratio of the panels. The reinforcing bar types obviously influenced the shear capacity of the panels, which reemphasizes the necessity of a customized model for GFRP-reinforced squat walls.

Structural level

Derivation—A simplified free-body diagram of a failed squat wall (Fig. 6(a)) is illustrated in Fig. 6(b). In compliance with ACI 374.2R-13,[58] the wall is loaded laterally and force equilibrium is achieved

$$P = F_t + F_{hw} + F_c \tag{15}$$

$$C = T + F_{vw} \tag{16}$$

$$P = T\frac{l_w - b_{be}}{h_w} + F_{hw}\frac{l_w - 2b_{be}}{2h_w}\cot\theta + F_{vw}\frac{l_w - b_{be}}{2h_w} \tag{17}$$

where P is the applied load; F_t and F_c are the resultant forces of the tension and compression boundary elements, respectively; F_{hw} and F_{vw} are the resultant forces of the web in the horizontal and vertical directions, respectively; C and T are the resistance of the boundary elements in compression and tension, respectively; l_w and h_w are the length and height of the wall, respectively; b_{be} is the width of the boundary element; and θ is the crack angle in degrees. Because the dowel action of GFRP reinforcing bars is negligible in a cracked plane,[12] the F_t term in Eq. (15) can be ignored. The

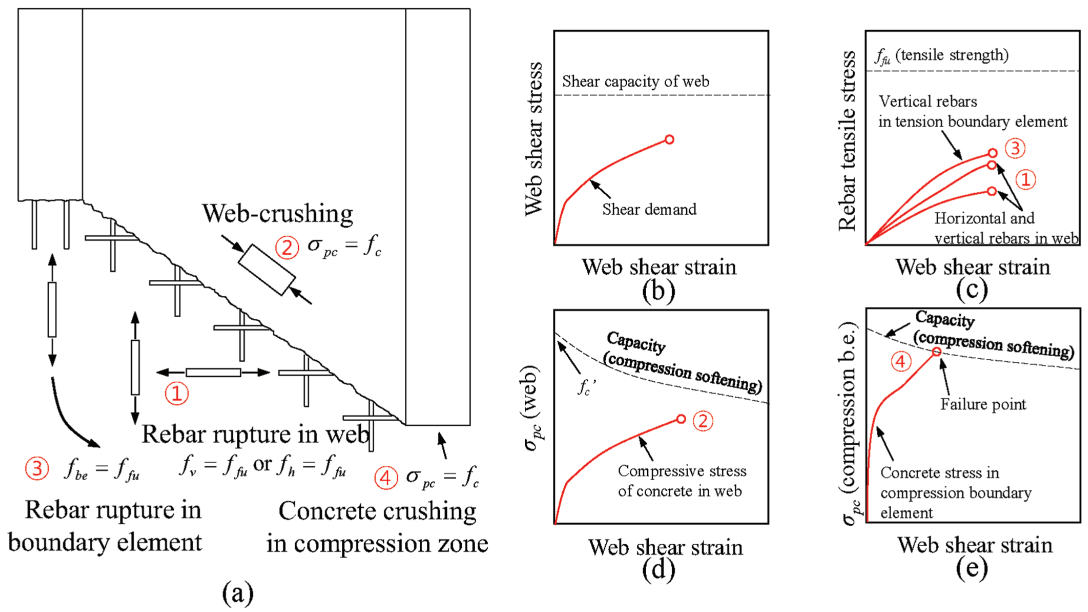

Fig. 7—Potential failure modes: (a) components; (b) stress-stain in web; (c) reinforcing bar stresses in web and tension boundary element; (d) concrete stress in web; and (e) concrete stress in compression boundary element.

horizontal force in the compression boundary element (F_c) is then obtained by combining Eq. (15) and (17)

$$F_c = P - F_{hw} = T\frac{l_w - b_{be}}{h_w} + F_{vw}\frac{l_w - b_{be}}{2h_w} + F_{hw}\left(\frac{l_w - 2b_{be}}{2h_w}\cot\theta - 1\right) \quad (18)$$

The organizational format of Eq. (18) explains the load-bearing mechanism of the squat wall in Fig. 1, corroborated by the failure pattern of test specimens No. 6 to 11 in Table 1: the horizontal force (F_c) in Fig. 6(b) would increase with an increase in the aspect ratio of the web (related to $h_w/(l_w - 2b_e)$ and $h_w/(l_w - b_e)$) and the vertical reinforcement in the web and the tension boundary element (concerned with F_{vw} and T). Likewise, Eq. (18) can account for the failure mode of the slender wall in Fig. 1: the F_c term decreases when the contribution of the vertical bars (F_{vw}) declines, which allows the progression of horizontal cracks along the web (that is, a precluded development of diagonal tension cracks). The linear elastic nature of GFRP reinforcing bars yields the succeeding expressions

$$F_{hw} = \rho_h E_f \varepsilon_h (l_w - 2b_e) t_w \cot\theta = \rho_h E_f \varepsilon_h A_{web} \cot\theta \quad (19)$$

$$F_{hv} = \rho_v E_f \varepsilon_v (l_w - 2b_e) t_w = \rho_v E_f \varepsilon_v A_{web} \quad (20)$$

$$T = \rho_{be} E_f \varepsilon_{be} b_{be} t_w = \rho_{be} E_f \varepsilon_{be} A_{be} = \rho_{be} E_f \varepsilon_v A_{be} \quad (21)$$

where ρ_h and ρ_v are the horizontal and vertical reinforcement ratios of the web, respectively; ρ_{be} is the reinforcement ratio of the boundary element; and ε_h, ε_v, and ε_{be} are the strains of the horizontal and vertical reinforcing bars and the boundary element, respectively. Because the web of a laterally loaded squat wall is subjected to uniform shear stress distributions,[59] the strain of the vertical reinforcing bars along the cracked plane (ε_v) may be equated with that of the boundary element (ε_{be}) transmitting axial forces (Fig. 6(b)). This approximation ($\varepsilon_v = \varepsilon_{be}$) is supported by experimentally measured strains.[8]

Failure criteria—Figure 7(a) depicts the possible failure modes of the squat wall model. The following is a succinct description of the individual cases.

1. *Rupture of GFRP reinforcing bars in the web*: When the stress of the vertical and horizontal reinforcing bars (f_v and f_h, respectively) is greater than the tensile strength of GFRP (f_{fu}), the reinforcing bars rupture. Contemplating that reinforcing bar strains at peak drift ratios in squat walls are generally smaller than the ultimate strain of commercially available GFRP reinforcing bars,[8,12] the occurrence of this failure mode may be uncommon.

2. *Web crushing*: Crushing failure of concrete in the web takes place if the principal compressive stress (σ_{pc}) reaches the softened concrete strength (f_c)

$$f_c = f_c' / (0.8 + 170\varepsilon_{pt}) \quad (22)$$

where ε_{pt} is the principal tensile strain of the concrete. Equation (22)[60] denotes the degradation of concrete with an increase in the maximum normal strain when subjected to mechanical loading; in other words, the shear deformation of the web under the lateral load (Fig. 6) raises the principal strain, thereby weakening the concrete resistance without regard to the type of reinforcement. As such, Eq. (22) can be used for both steel- and FRP-reinforced concrete members.[61]

3. *Rupture of GFRP reinforcing bars in the tension boundary element*: Reinforcing bars will rupture when their stress (f_{be}) equals the tensile strength (f_{fu}), which depends upon the amount of longitudinal reinforcing bars in the tension boundary element. Conventionally speaking, the tension boundary element of a shear wall transmits axial forces[62]; thus, stress interactions between normal and inclined components are negligible.

4. *Concrete crushing in the compression boundary element*: The combined shear and compression forces in

the compression boundary element at the reference point associated with moment equilibrium (Fig. 6(b)) increase concrete stresses and prompt crushing failure ($\sigma_{pc} = f_c$). This failure type is frequently observed in squat walls tested in laboratories.[8,16]

The notional explication of these failure modes is provided in Fig. 7(b) to (e). When the squat wall is loaded laterally, the stress and strain of the web increase in a steady manner (Fig. 7(b)). The stress states of the reinforcing bars and concrete in the web and the boundary elements are computed as detailed in the previous section, and those are compared against the aforementioned failure criteria. The shear deformation of the web causes the elongation of the horizontal and vertical reinforcing bars (Fig. 7(c)) as well as the compression of the concrete (Fig. 7(d)). The lateral load also exerts axial tension and compression to the boundary elements (Fig. 7(c) and (e)). As drawn in Fig. 7(e), the shear-compression-combined action in the compression boundary element augments the concrete stress and can accelerate the development of the principal stress, resulting in the crushing of the concrete that is reported in laboratory research.[8,16]

Implementation—The previously described model is solved with a procedure recapitulated in Fig. 8. Numerical iterations are necessary to determine the failure mode and load-bearing capacity of the squat wall:

Step 1: The geometric and material properties of the wall structure are collected as input parameters, including concrete and GFRP reinforcing bars

Step 2: An initial shear strain in the web (γ) is assumed with a small fraction of the concrete cracking strain (γ = 0.0005 was chosen for the present study). Afterward, in accordance with the Modified Compression Field Theory,[53] the constituent strains of the concrete (ε_{pt} and ε_{pc}, in which ε_{pc} is the strain corresponding to the principal compressive stress σ_{pc}) and GFRP (ε_h and ε_v) are calculated. Each of the four possible failure modes defined earlier is checked, belonging to the assumed shear strain.

Step 3: Upon obtaining the strains in the web from Step 2, the forces in the boundary elements are computed (C, F_c, and T in Eq. (16), (18), and (21), respectively). For the failure of the tension boundary element, the tensile force T is compared with the ultimate capacity of the reinforcing bar ($\rho_{be} f_{fu} b_{be} t_w$). Regarding the compression boundary element, the maximum shear stress attained from the Modified Compression Field Theory involving the compression force C is multiplied by the cross-sectional area of the boundary element to ascertain the horizontal resistance F_c, which is evaluated against the shear strength of the element.

Step 4: The stresses and resultant forces from Step 3 are appraised per the criteria established in Fig. 7(a). If a failure condition is not satisfied, the shear strain γ is increased ($\gamma_{i+1} = \gamma_i + \Delta\gamma$) and Steps 2 through 4 are repeated until a specific failure mode is found. Next, the nominal capacity of the squat wall (V_n) is quantified.

Verification—The proposed approach is validated employing the test data enumerated in Table 1. As witnessed in the laboratory, the predicted failure mode of the squat wall specimens was concrete crushing in the compression boundary element (Fig. 7(a)). Figure 9(a) assesses the

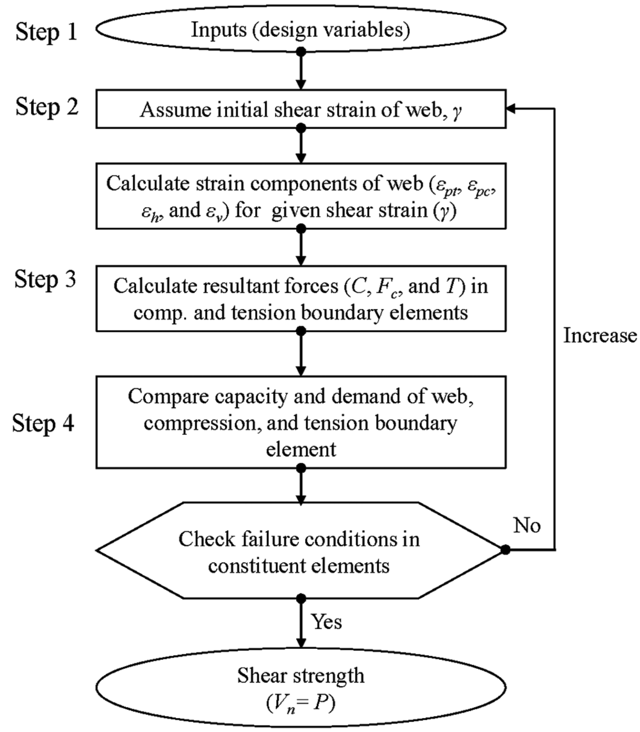

Fig. 8—Flowchart for implementation of proposed model.

predictability of the nominal shear capacity (V_n). The capacity ratio of V_{test}/V_n varied from 0.82 to 1.16, with a mean and standard deviation of 1.002 and 0.134, respectively. On the strain of the horizontal GFRP reinforcing bars in the web at the specimens' peak loads, the theoretical values were comparable to the measured strain range.[8] The strain limit of 0.004 in ACI.440.1R-15[12] served as the lower bound of the experimental strains (Fig. 9(b)), implying that this limit should be kept in the design of GFRP-reinforced squat walls.

DESIGN RECOMMENDATIONS

In an effort to improve the prediction of shear capacity in GFRP-reinforced walls, rational recommendations are made. Additionally, a new classification is proposed to definitize the taxonomy of squat and slender walls with an emphasis on not only wall geometries but also other attributes such as reinforcement ratios.

Proposed revision

The shear capacity of the squat wall is composed of F_c and F_{hw} (Eq. (18)). From a traditional design standpoint,[5,11,12] the F_c and F_{hw} terms can be regarded as V_c and V_f in Eq. (1), respectively. Given that the shear-resisting mechanism of the compression boundary element (Fig. 6(b)) differs from the mechanism of conventional reinforced concrete beams accompanying dowel action and aggregate interlock, the existing expression of V_c needs to be revised. Figure 10 instantiates a relationship between the capacity ratio of V_{test}/V_n and the proportion of the concrete strength ($\alpha f_c'$, where α is the fraction factor): conforming to the recommendation of prior research,[63] the shear stress range of the walls at failure was represented by $\alpha f_c'$ with an upper limit of $0.3 f_c'$. For comparison, the V_c term in Fig. 10(a) was set to be a product of the proportional stress and the cross-sectional area of

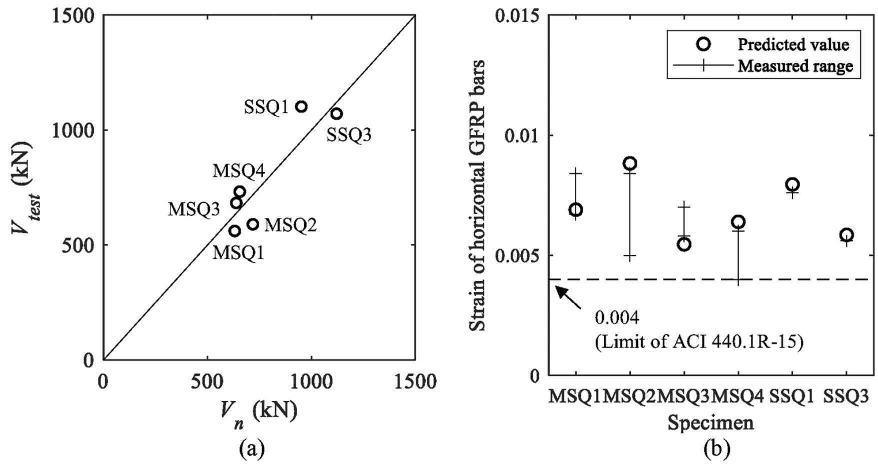

Fig. 9—Validation of proposed model: (a) shear capacity; and (b) strain of horizontal reinforcing bars at peak load. (Note: 1 kN = 0.225 kip.)

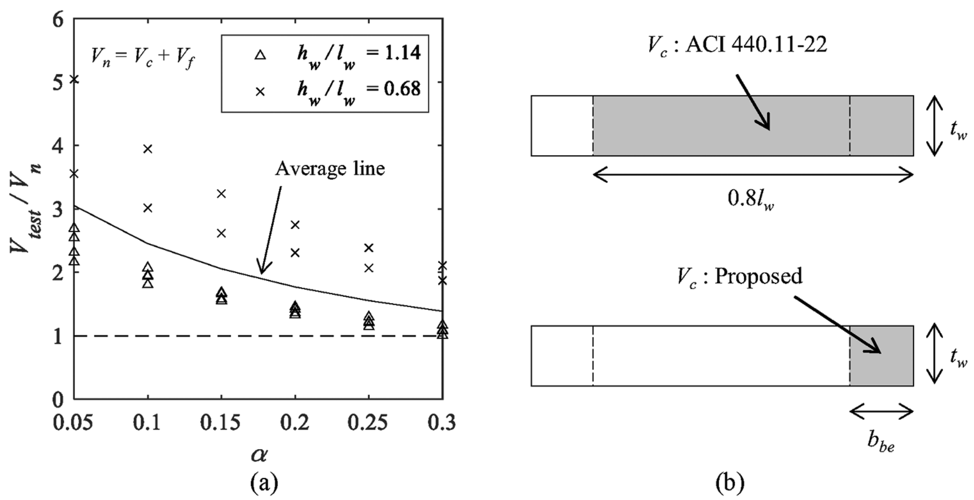

Fig. 10—Sensitivity analysis of stress fraction factor: (a) variation; and (b) effective cross-sectional area for shear resistance of concrete.

the compression boundary element ($V_c = \alpha f_c' b_{be} t_w$). Within the scope of interest ($0.05 \leq \alpha \leq 0.3$), the capacity ratio gradually diminished with the fraction factor. The extent of discrepancy in the ratio was the least at $\alpha = 0.3$ and the corresponding average value of $V_{test}/V_n = 1.39$ was less than the value of 2.45 at $\alpha = 0.1$ ($0.1f_c'$ is equivalent to the current design expression of ACI 440.11-22[11]). The enhanced capacity ratio with $\alpha = 0.3$ is attributed to the fact that the shear stress of $0.3f_c'$ generated higher resistance relative to the stress stemming from ACI 440.11-22[11] and that the use of the compression boundary element ($b_{be}t_w$, Fig. 10(b)) in the cracked squat wall (Fig. 6) was more realistic than the use of the entire web in the existing design approaches.[5,11] Consequently, Eq. (23) is suggested for Eq. (1)

$$V_c = 0.3f_c' b_{be} t_w = 0.3f_c' \beta l_w t_w \tag{23}$$

where β is the area ratio of the boundary element to the wall ($\beta = (b_{be}t_w)/(l_w t_w)$). The nominal shear resistance of the squat wall is, therefore, written in conjunction with Eq. (5) and (23)

$$V_n = V_c + V_f = 0.3f_c'\beta l_w t_w + (0.004E_f)A_{fv}d/s \leq k_2 f_c'^{0.5} l_w t_w \tag{24}$$

It should be noted that the allowable strain limit of $\Omega = 0.004$ in Eq. (6) was not modified as articulated in the Verification section.

Determination of failure modes

Unlike the traditional definition of squat walls based only on an aspect ratio, a new criterion may be established by manipulating the analytical model to encompass the unique features of GFRP-reinforced concrete walls. This attempt imparts technical merits because the reinforcing schemes of shear walls with steel and GFRP reinforcing bars are not the same. Rearranging Eq. (18) to (21) yields Eq. (25), which manifests the strains of the horizontal and vertical GFRP reinforcing bars (ε_h, ε_v, and ε_{be})

$$F_c = \rho_{be} E_f \varepsilon_{be} A_{be} \frac{l_w - b_{be}}{h_w} + \rho_v E_f \varepsilon_v A_{web} \frac{l_w - b_{be}}{2h_w} + \rho_h E_f \varepsilon_h A_{web} \cot\theta \left(\frac{l_w - 2b_{be}}{2h_w} \cot\theta - 1 \right) \tag{25}$$

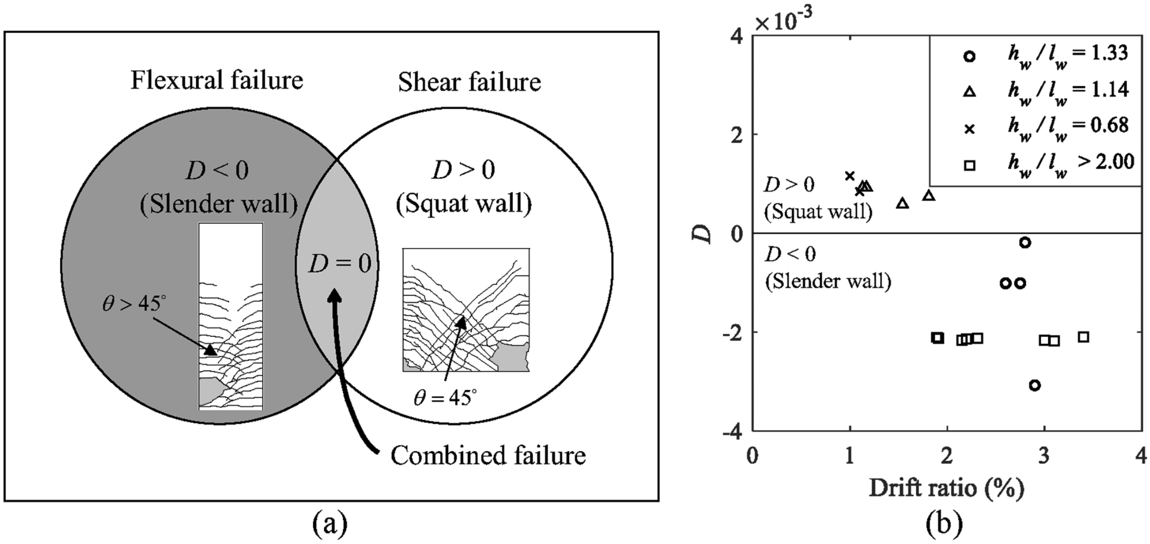

Fig. 11—Determination of failure modes: (a) Venn diagram; and (b) experimental verification.

where A_{be} and A_{web} are the cross-sectional areas of the boundary element and the web, respectively ($A_{be} = b_{be}t_w$ and $A_{web} = (l_w - 2b_{be})t_w$). Aligning with the cracked web of the squat wall shown in Fig. 6, the angle θ may be assumed to be 45 degrees and the strain compatibility condition ($\cot^2\theta = (\varepsilon_h+\varepsilon_{pc})/(\varepsilon_v+\varepsilon_{pc})$ in Vecchio and Collins[53]) enables

$$\varepsilon_\eta = (\varepsilon_v + \varepsilon_{pc})\cot\theta^2 - \varepsilon_{pc} = \varepsilon_v \tag{26}$$

Taking the previously discussed uniform stress distribution of $\varepsilon_v = \varepsilon_{be}$ and the strain limit of 0.004 stipulated in ACI 440.1R-15,[12]

$$\varepsilon_\eta = \varepsilon_v = \varepsilon_{be} = 0.004 \tag{27}$$

Then, Eq. (25) is restated as

$$F_c = 0.25\left(\begin{array}{l}\rho_{be} f_{fu} A_{be}\dfrac{l_w - b_{be}}{h_w} + \rho_v f_{fu} A_{web}\dfrac{l_w - b_{be}}{2h_w} + \\ \rho_h f_{fu} A_{web}\left(\dfrac{l_w - 2b_{be}}{2h_w} - 1\right)\end{array}\right) \tag{28}$$

Dividing Eq. (28) by $f_{fu}A_w$, in which A_w is the gross cross-sectional area of the wall ($A_w = l_w t_w = A_{web} + 2A_{be}$), provides a failure determinant index (D)

$$D = \frac{F_c}{f_{fu}A_w} = 0.25\left(\begin{array}{l}\rho_{be}\dfrac{A_{be}}{A_w}\dfrac{l_w - b_{be}}{h_w} + \rho_v\dfrac{A_{web}}{A_w}\dfrac{l_w - b_{be}}{2h_w} + \\ \rho_h\dfrac{A_{web}}{A_w}\left(\dfrac{l_w - 2b_{be}}{2h_w} - 1\right)\end{array}\right) \tag{29}$$

If this nondimensional index is positive ($D > 0$), the equilibrium condition depicted in Fig. 6(b) is satisfied; scilicet, the direction of the resultant force in the compression boundary element (F_c) is opposite to the applied load P. On the other hand, if the index is negative ($D < 0$), the direction of these forces is the same; hence, the assumed crack angle of θ = 45 degrees in Eq. (26) and (29) becomes invalid and the angle has to be increased to comply with the equilibrium condition (θ > 45 degrees). In that circumstance, the crack pattern of the wall conforms to the archetypal pattern of a slender wall (Fig. 11(a), inset). Equation (30) is thus adduced to discern the failure mode of structural walls with GFRP reinforcement

$$\begin{array}{l} D > 0 \rightarrow \text{squat walls with shear failure} \\ D = 0 \rightarrow \text{transition with combined shear-flexural failure} \\ D < 0 \rightarrow \text{slender walls with flexural failure} \end{array} \tag{30}$$

Allowing for the constituent terms in Eq. (29), GFRP-reinforced concrete walls with an aspect ratio of less than $h_w/l_w = 1.5$ can demonstrate flexural failure such as in the case of the slender category if their reinforcement ratios (ρ_{be}) are sufficiently low to precipitate horizontal tensile cracks. For instance, Fig. 11(b) displays the failure mode of the laboratory-tested squat walls listed in Table 1 as well as that of slender walls possessing aspect ratios greater than $h_w/l_w = 2.0$.[64,65] The specimens with an aspect ratio of $h_w/l_w = 0.68$ and 1.14 and a reinforcement ratio of $\rho_{be} = 4.48$ failed in shear ($D > 0$), whereas the specimens with $h_w/l_w = 1.33$ were positioned in the $D < 0$ domain, which matches the flexural failure observed in the laboratory and proves that the aspect ratio of structural walls is not the only factor that divides the boundary between the squat and slender categories.

Vertical reinforcement in boundary elements

A characteristic reinforcement ratio in the boundary elements ($\rho_{be,c}$) may be derived from the failure determinant function, which serves as a medium to adjust the failure mode of GFRP-reinforced concrete walls. At $D = 0$ in Eq. (29), the characteristic reinforcement ratio is specified to be

$$\rho_{be,c} = \left(\rho_h\left(\frac{2h_w - l_w + 2b_{be}}{2(l_w - b_{be})}\right) - 0.5\rho_v\right)\frac{(l_w - 2b_{be})t_w}{b_{be}t_w} \tag{31}$$

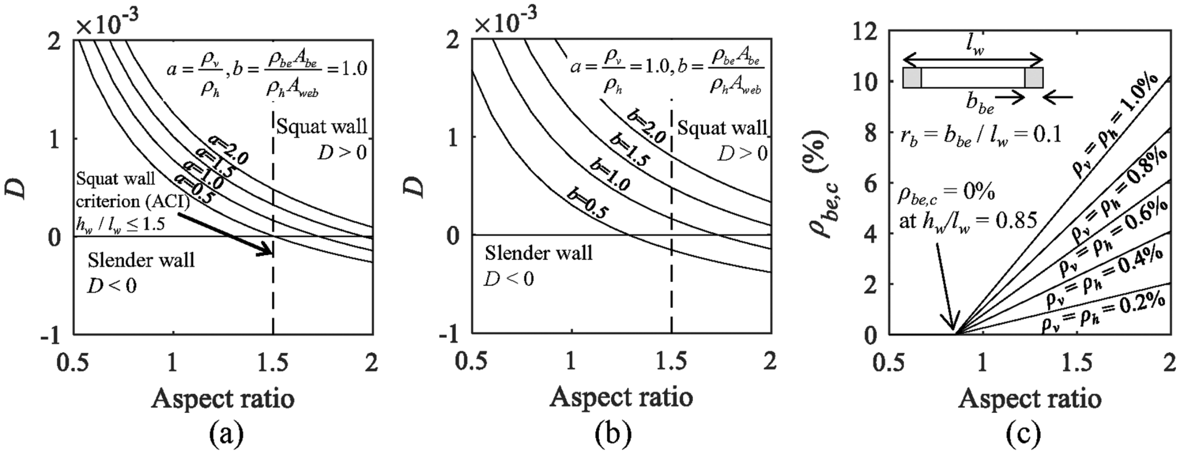

Fig. 12—Parametric analysis: (a) vertical reinforcement ratio in web; (b) longitudinal reinforcement ratio in boundary elements; and (c) characteristic vertical reinforcement ratio in boundary elements.

Equation (31) is a demarcation that apprehends whether a wall with GFRP reinforcing bars potentially fails in shear or flexure. If a reinforcement ratio in the boundary elements is greater than the characteristic ratio ($\rho_{be,c} < \rho_{be}$), shear dominates as in the failure of a squat wall. For an engineering project, practitioners can tailor ρ_{be} to accomplish an intended failure of the subject wall. A concise version of Eq. (31) is offered by letting $r_b = b_{be}/l_w$ and $a_r = h_w/l_w$ under a usual reinforcing scheme of $\rho_h = \rho_v$ in the web

$$\rho_{be,c} = \rho_h\left(\frac{a_r - 1 + 1.5\,r_b}{1 - r_b}\right)(1/r_b - 2) \tag{32}$$

Parametric studies

The implications of geometric and reinforcing configurations for the failure of GFRP-reinforced concrete walls are visible in Fig. 12(a) through (c). A typical wall was selected (Specimen No. 8 in Table 1) for parametric investigations and its properties were used as the defaults, unless otherwise stated. Figure 12(a) exhibits the influence of a relative amount in placing vertical and horizontal reinforcing bars (ρ_v/ρ_h). With the increased aspect ratio, the determinant index (D) dwindled and the failure mode of the wall tended to shift from shear to flexure. The response curves were also affected by the vertical reinforcement ratio ρ_v. Specifically, the placement of more vertical reinforcing bars retarded the transition of the failure mode because the shear friction of the wall ascended, so the load-bearing mechanism of the squat wall was preserved. The transformational threshold of $D = 0$ that distinguishes the failure mode of the walls enveloped aspect ratios from $h_w/l_w = 1.5$ to 2.0. This finding explicates the reason why a single aspect ratio was not suited for defining a limit between squat and slender walls, which was inconclusively argued in the structural concrete community.[7-9] The reinforcement ratio of the boundary elements (ρ_{be}) was influential in altering the failure mode of the walls (Fig. 12(b)). Even though the variation trend of D was similar to the case of Fig. 12(a), the impact of ρ_{be} was prominent in comparison with ρ_v; namely, depending upon the value of ρ_{be}, a GFRP-reinforced concrete wall with $h_w/l_w > 2.0$ can still fail in shear as in the occasion of a squat wall. The growth of the characteristic reinforcement ratio ($\rho_{be,c}$) comprising a representative boundary element size of $r_b = 0.1$ is plotted in Fig. 12(c). The elevated slope of the characteristic ratio ($\rho_{be,c}$) with the reinforcement ratios of the web (ρ_v and ρ_h) points out that the balanced failure condition of the wall ($D = 0$) necessitated more reinforcing bars as its aspect ratio rose, reaffirming the significance of GFRP amounts in classifying squat and slender walls. It is, however, worth noting that the reliance of the web reinforcement ratios disappeared when the aspect ratio was below $h_w/l_w = 0.85$: the structural member was sorted into a squat wall that failed in shear, regardless of the reinforcement ratios.

SUMMARY AND CONCLUSIONS

This paper has dealt with mechanics-based analytical modeling to construe the shear behavior of glass fiber-reinforced polumer (GFRP)-reinforced squat walls when subjected to lateral loading. Through a rigorous review of existing design articles in tandem with experimental data, the limitations of current specifications were explored and the need for developing amended guidelines arose. Two-phase examinations, from local and global points of view, bring to light the influence of reinforcement type on the response of squat walls and their failure criteria as regards various stress states in structural components. A rational design proposal was made, coupled with a novel determinant index assorting load-bearing walls into squat and slender categories. Moreover, a characteristic reinforcement was rendered to assist engineering professionals in allocating architectural elements. The following are concluded:

- The provisions of ACI CODE-440.11-22[11] underestimated the shear capacity of GFRP-reinforced squat walls, particularly noticeable when an aspect ratio was as low as $h_w/l_w = 0.68$, owing to the empirical nature of the equations originating from flexure-shear-combined responses.
- The behavioral differences of squat walls with steel and GFRP reinforcing bars were evident in terms of failure characteristics and shear stress developments. The

source of these discrepancies was reinforcing amounts, tension-stiffening mechanisms, and material properties.

- The mechanics-based model ameliorated the accuracy of predicting the shear capacity of GFRP-reinforced squat walls and led to the derivation of revised expressions, constituted with the cross-sectional area of the compression boundary element and the maximum allowable reinforcing bar strain of 0.004.
- Contrary to the prevalent methodologies relying on ambiguous aspect ratios, the determinant index demystified the classification of squat walls by using the geometric and reinforcing attributes of the walls.
- The suggested characteristic reinforcement ratio would facilitate the adjustment of failure modes in GFRP-reinforced concrete walls involving an aspect ratio greater than $h_w/l_w = 0.85$, below which shear would be the dominant failure mode irrespective of reinforcing schemes in the boundary elements.

AUTHOR BIOS

Ju-Hyung Kim *is a Postdoctoral Fellow in the Department of Civil Engineering at the University of Colorado Denver, Denver, CO. He received his BE, MS, and PhD from the Department of Architecture and Architectural Engineering at Seoul National University, Seoul, South Korea. His research interests include seismic design, performance evaluation, and statistical analysis of reinforced concrete structures.*

Yail J. Kim, *FACI, is President of the Bridge Engineering Institute, An International Technical Society, and a Professor in the Department of Civil Engineering at the University of Colorado Denver. He is Chair of ACI Subcommittee 440-I, FRP-Prestressed Concrete; past Chair of ACI Committee 345, Bridge Construction and Preservation; and a member of ACI Committees 342, Evaluation of Concrete Bridges and Bridge Elements; 377, Performance-Based Structural Integrity & Resilience of Concrete Structures; 440, Fiber-Reinforced Polymer Reinforcement; and Joint ACI-ASCE Committee 343, Concrete Bridge Design. He received the ACI Chester Paul Siess Award for Excellence in Structural Research in 2019. His research interests include advanced composite materials for rehabilitation, structural informatics, complex systems, and science-based structural engineering including statistical, interfacial, and quantum physics.*

Hong-Gun Park, *FACI, is a Professor in the Department of Architecture & Architectural Engineering at Seoul National University. He received his BE and MS in architectural engineering from Seoul National University and his PhD in civil engineering from the University of Texas at Austin, Austin, TX. His research interests include numerical analysis, earthquake design of reinforced concrete, and composite structures.*

ACKNOWLEDGMENTS

This research is in part supported by the U.S. Department of Transportation through the Mountain-Plains Consortium, for which the authors are grateful. Technical contents presented herein are based on the opinion of the writers, and do not necessarily represent those of others.

REFERENCES

1. Nawy, E. G., *Reinforced Concrete: A Fundamental Approach*, Pearson, Upper Saddle River, NJ, 2008.

2. Robazza, B. R.; Yang, T. Y.; Brzev, S.; Elwood, K. J.; Anderson, D. L.; and McEwen, W., "Response of Slender Reinforced Masonry Shear Walls with Flanged Boundary Elements under In-Plane Lateral Loading: An Experimental Study," *Engineering Structures*, V. 190, 2019, pp. 389-409. doi: 10.1016/j.engstruct.2019.04.035

3. Xu, G., and Li, A., "Research on the Response of Concrete Cavity Shear Wall under Lateral Load," *Structural Design of Tall and Special Buildings*, V. 28, No. 3, 2019, p. e1577. doi: 10.1002/tal.1577

4. Zhang, J.; Li, X.; Cao, W.; and Yu, C., "Seismic Behavior of Composite Shear Walls Incorporating High-Strength Materials and CFST Boundary Elements," *Engineering Structures*, V. 220, 2020, p. 110994. doi: 10.1016/j.engstruct.2020.110994

5. ACI Committee 318, "Building Code Requirements for Structural Concrete (ACI 318-19) and Commentary (ACI 318R-19) (Reapproved 2022)," American Concrete Institute, Farmington Hills, MI, 2019, 624 pp.

6. Parra, P. F., and Moehle, J. P., "Effects of Strain Gradients in the Onset of Global Buckling in Slender Walls Due to Earthquake Loading," *Bulletin of Earthquake Engineering*, V. 18, No. 7, 2020, pp. 3205-3221. doi: 10.1007/s10518-020-00821-3

7. Zhou, Y.; Zheng, S.; Chen, L.; Long, L.; and Wang, B., "Experimental Investigation into the Seismic Behavior of Squat Reinforced Concrete Walls Subjected to Acid Rain Erosion," *Journal of Building Engineering*, V. 44, 2021, p. 102899. doi: 10.1016/j.jobe.2021.102899

8. Shabana, I.; Farghaly, A. S.; and Benmokrane, B., "Effect of Axial Load and Web Reinforcement Ratio on Seismic Behavior of Glass Fiber-Reinforced Polymer-Reinforced Concrete Squat Walls," *ACI Structural Journal*, V. 118, No. 4, July 2021, pp. 109-121.

9. Hosseini, S. M.; Yekrangnia, M.; and Vatani Oskouei, A., "Effect of Spiral Transverse Bars on Structural Behavior of Concrete Shear Walls Reinforced with GFRP Bars," *Journal of Building Engineering*, V. 55, 2022, p. 104706. doi: 10.1016/j.jobe.2022.104706

10. Nanni, A.; De Luca, A.; and Zadeh, H. J., *Reinforced Concrete with FRP Bars: Mechanics and Design*, CRC Press, Boca Raton, FL, 2014.

11. ACI Committee 440, "Building Code Requirements for Structural Concrete Reinforced with Glass Fiber-Reinforced Polymer (GFRP) Bars—Code and Commentary (ACI CODE-440.11-22)," American Concrete Institute, Farmington Hills, MI, 2022, 260 pp.

12. ACI Committee 440, "Guide for the Design and Construction of Structural Concrete Reinforced with Fiber-Reinforced Polymer (FRP) Bars (ACI 440.1R-15)," American Concrete Institute, Farmington Hills, MI, 2015, 88 pp.

13. Belay, A., and Wondimu, T., "Seismic Performance Evaluation of Steel and GFRP Reinforced Concrete Shear Walls at High Temperature," *Journal of Engineering and Applied Sciences (Asian Research Publishing Network)*, V. 70, 2023, p. 4

14. Mohamed, N.; Farghaly, A. S.; Benmokrane, B.; and Neale, K. W., "Flexure and Shear Deformation of GFRP-Reinforced Shear Walls," *Journal of Composites for Construction*, ASCE, V. 18, No. 2, 2014, p. 04013044. doi: 10.1061/(ASCE)CC.1943-5614.0000444

15. Ghazizadeh, S., and Cruz-Noguez, C. A., "Damage-Resistant Reinforced Concrete Low-Rise Walls with Hybrid GFRP-Steel Reinforcement and Steel Fibers," *Journal of Composites for Construction*, ASCE, V. 22, No. 2, 2018, p. 04018002. doi: 10.1061/(ASCE)CC.1943-5614.0000834

16. Shabana, I.; Farghaly, A. S.; and Benmokrane, B., "Earthquake Response of GFRP-Reinforced Concrete Squat Walls with Aspect Ratio of 1.14 and 0.68," *Engineering Structures*, V. 252, 2022, p. 113556. doi: 10.1016/j.engstruct.2021.113556

17. Deger, Z. T., and Basdogan, C., "Empirical Expressions for Deformation Capacity of Reinforced Concrete Structural Walls," *ACI Structural Journal*, V. 116, No. 6, Nov. 2019, pp. 53-61. doi: 10.14359/51716806

18. Siam, A.; Ezzeldin, M.; and El-Dakhakhni, W., "Machine Learning Algorithms for Structural Performance Classifications and Predictions: Application to Reinforced Masonry Shear Walls," *Structures*, V. 22, 2019, pp. 252-265. doi: 10.1016/j.istruc.2019.06.017

19. Arafa, A.; Farghaly, A. S.; and Benmokrane, B., "Effect of Web Reinforcement on the Seismic Response of Concrete Squat Walls Reinforced with Glass-FRP Bars," *Engineering Structures*, V. 174, 2018, pp. 712-723. doi: 10.1016/j.engstruct.2018.07.092

20. Arafa, A.; Farghaly, A. S.; and Benmokrane, B., "Experimental Behavior of GFRP-Reinforced Concrete Squat Walls Subjected to Simulated Earthquake Load," *Journal of Composites for Construction*, ASCE, V. 22, No. 2, 2018, p. 04018003. doi: 10.1061/(ASCE)CC.1943-5614.0000836

21. Architectural Institute of Japan, "Load-Deflection Characteristics of Nuclear Reactor Building Structures: Parts 8-9-10," *Summaries of Technical Papers, Structural Division*, V. 58, 1985. (in Japanese)

22. AIJ, "Load-Deflection Characteristics of Nuclear Reactor Building Structures: Parts 37-38-39-40," *Summaries of Technical Papers of Annual Meeting, B, Structures I*, Architectural Institute of Japan, Tokyo, Japan, 1985. (in Japanese)

23. Architectural Institute of Japan, "Load-Deflection Characteristics of Nuclear Reactor Building Structures: Parts 21-22," *Summaries of Technical Papers, Structural Division*, V. 59, 1986. (in Japanese)

24. AIJ, 1986b. "Load-Deflection Characteristics of Nuclear Reactor Building Structures: Parts 59-60-61," *Summaries of Technical Papers of Annual Meeting, B, Structures I*, Architectural Institute of Japan, Tokyo, Japan, 1986. (in Japanese)

25. AIJ, "Load-Deflection Characteristics of Nuclear Reactor Building Structures: Parts 62-63," *Summaries of Technical Papers of Annual Meeting, B, Structures I*, Architectural Institute of Japan, Tokyo, Japan, 1986. (in Japanese)

26. Antebi, J.; Utku, S.; and Hansen, R. J., "The Response of Shear Walls to Dynamic Loads," Massachusetts Institute of Technology, Cambridge, MA, 1960.
27. Bouchon, M.; Orbovic, N.; and Foure, N., "Tests on Reinforced Concrete Low-Rise Shear Walls under Static Cyclic Loading," *Proceedings of the Thirteenth World Conference on Earthquake Engineering*, Vancouver, BC, Canada, 2004, pp. 1-10.
28. Gao, X., "Framed Shear Walls under Cyclic Loading," PhD dissertation, University of Houston, Houston, TX, 1999.
29. Hidalgo, P. A.; Jordan, R. M.; and Martinez, M. P., "An Analytical Model to Predict the Inelastic Seismic Behavior of Shear Wall, Reinforced Concrete Structures," *Engineering Structures*, V. 24, No. 1, 2002, pp. 85-98. doi: 10.1016/S0141-0296(01)00061-X
30. Hirosawa, M., "Past Experimental Results on Reinforced Concrete Shear Walls and Analysis on Them," Building Research Institute, Ministry of Construction, Tokyo, Japan, 1975, 277 pp. (in Japanese)
31. Kabeyasawa, T., and Somaki, T., "Reinforcement Details for Reinforced Concrete Shear Walls with Thick Panel," *Transactions of the Japan Concrete Institute*, V. 7, 1985, pp. 369-372. (in Japanese)
32. Kim, J.-H., and Park, H.-G., "Shear and Shear-Friction Strengths of Squat Walls with Flanges," *ACI Structural Journal*, V. 117, No. 6, Nov. 2020, pp. 269-280. doi: 10.14359/51728075
33. Kim, S.-H., and Park, H.-G., "Shear Strength of Reinforced Concrete Wall with 700 MPa Shear Reinforcement," *ACI Structural Journal*, V. 118, No. 2, Mar. 2021, pp. 167-181.
34. Kim, J.-H., and Park, H.-G., "Shear Strength of Flanged Squat Walls with 690 MPa Reinforcing Bars," *ACI Structural Journal*, V. 119, No. 2, Mar. 2022, pp. 209-220.
35. Liu, X.; Burgueno, R.; Egleston, E.; and Hines, E. M., "Inelastic Web Crushing Performance Limits of High-Strength-Concrete Structural Wall-Single Wall Test Program," Report No. CEE-RR-2009/03, Michigan State University, East Lansing, MI, 2009.
36. Luna, B. N.; Rivera, J. P.; and Whittaker, A. S., "Seismic Behavior of Low-Aspect Ratio Reinforced Concrete Shear Walls," *ACI Structural Journal*, V. 112, No. 5, Sept.-Oct. 2015, pp. 593-604. doi: 10.14359/51687709
37. Maier, J., and Thurlimann, B., 1985, "Bruchversuche an stahlbetonscheiben," Institut für Baustatik und Konstruktion, Eidgenössische Technische Hochschule (ETH) Zürich, Switzerland, 130 pp. (in German)
38. Massone, L. M.; Orakcal, K.; and Wallace, J. W., "Modeling of Squat Structural Walls Controlled by Shear," *ACI Structural Journal*, V. 106, No. 5, Sept.-Oct. 2009, pp. 646-655.
39. Mo, Y. L., and Chan, J., "Behavior of Reinforced-Concrete Framed Shear Walls," *Nuclear Engineering and Design*, V. 166, No. 1, 1996, pp. 55-68. doi: 10.1016/0029-5493(96)01244-7
40. Mohammadi-Doostdar, H., "Behavior and Design of Earthquake Resistant Low-Rise Shear Walls," University of Ottawa, Ottawa, ON, Canada, 1994.
41. Oesterle, R. G.; Aristizabal-Ochoa, J. D.; Fiorato, A. E.; Russell, H. G.; and Corely, W. G., 1979, "Earthquake Resistant Structural Walls-Tests of Isolated Walls-Phase II," Construction Technology Laboratories, Portland Cement Association, Skokie, IL.
42. Ogata, K., and Kabeyasawa, T., "Experimental Study on the Hysteretic Behavior of Reinforced Concrete Shear Walls under the Loading of Different Moment-to-Shear Ratios," *Transactions of the Japan Concrete Institute*, V. 6, 1984, pp. 717-724.
43. Park, H.-G.; Baek, J.-W.; Lee, J.-H.; and Shin, H.-M., "Cyclic Loading Tests for Shear Strength of Low-Rise Reinforced Concrete Walls with Grade 550 MPa Bars," *ACI Structural Journal*, V. 112, No. 3, May-June 2015, pp. 299-310. doi: 10.14359/51687406
44. Pilette, F. C., "Behavior of Earthquake Resistant Squat Shear Walls," MS thesis, University of Ottawa, Ottawa, ON, Canada, 1987.
45. Rothe, D., "Untersuchungen zum nichtlinearen Verhalten von stahlbeton wandschieben unter erdebenbeanspruchung," PhD dissertation, Fachbereich Konstruktiver Ingenieurbau, der Technischen Hochschule Darmstadt, Darmstadt, Germany, 1992, 161 pp. (in German)
46. Saito, H.; Kikuchi, R.; Kanechika, M.; and Okamoto, K., "Experimental Study on the Effect of Concrete Strength on Shear Wall Behavior," *Proceedings of the Tenth International Conference on Structural Mechanics in Reactor Technology*, Anaheim, CA, 1989.
47. Salonikios, T. N.; Kappos, A. J.; Tegos, I. A.; and Penelis, G. G., "Cyclic Load Behavior of Low-Slenderness Reinforced Concrete Walls: Design Basis and Test Results," *ACI Structural Journal*, V. 96, No. 4, July-Aug. 1999, pp. 649-660.
48. Sato, S.; Ogata, Y.; Yoshizaki, S.; Kanata, K.; Yamaguchi, T.; Nakayama, T.; Inada, Y.; and Kadoriku, J., "Behavior of Shear Wall Using Various Yield Strength of Reinforcing Bar, Part 1: An Experimental Study," *Proceedings of the Tenth International Conference on Structural Mechanics in Reactor Technology*, Anaheim, CA, 1989.
49. Seki, M.; Kobayashi, J.; Shibata, A.; Kubo, T.; Taira, T.; and Akino, K., "Restoring Force Verification Test on RC Shear Wall," *Proceedings of the Thirteenth International Conference on Structural Mechanics in Reactor Technology*, Porto Alegre, Brazil, 1995.
50. Synge, A. J., "Ductility of Squat Shear Walls," Report No. 80-8, University of Canterbury, Christchurch, New Zealand, 1980.
51. Teng, S., and Chandra, J., "Cyclic Shear Behavior of High Strength Concrete Structural Walls," *ACI Structural Journal*, V. 113, No. 6, Nov.-Dec. 2016, pp. 1335-1345. doi: 10.14359/51689158
52. Vecchio, F. J.; Collins, M. P.; and Aspiotis, J., "High-Strength Concrete Elements Subjected to Shear," *ACI Structural Journal*, V. 91, No. 4, July-Aug. 1994, pp. 423-433.
53. Vecchio, F. J., and Collins, M. P., "The Modified Compression Field Theory for Reinforced Concrete Elements Subjected to Shear," *ACI Journal Proceedings*, V. 83, No. 2, Mar.-Apr. 1986, pp. 219-231.
54. Bischoff, P. H., and Paixao, R., "Tension Stiffening and Cracking of Concrete Reinforced with Glass Fiber Reinforced Polymer (GFRP) Bars," *Canadian Journal of Civil Engineering*, V. 31, No. 4, 2004, pp. 579-588. doi: 10.1139/l04-025
55. Miglietta, P. C.; Grasselli, G.; and Bentz, E. C., "Finite/Discrete Element Model of Tension Stiffening in GFRP Reinforced Concrete," *Engineering Structures*, V. 111, 2016, pp. 494-504. doi: 10.1016/j.engstruct.2015.12.037
56. Kharal, Z., and Sheikh, S., "Tension Stiffening and Cracking Behavior of Glass Fiber- Reinforced Polymer-Reinforced Concrete," *ACI Structural Journal*, V. 114, No. 2, Mar.-Apr. 2017, pp. 299-310. doi: 10.14359/51689420
57. Razaqpur, A. G.; Svecova, D.; and Cheung, M. S., "Rational Method for Calculating Deflection of Fiber-Reinforced Polymer Reinforced Beams," *ACI Structural Journal*, V. 97, No. 1, Jan.-Feb. 2000, pp. 175-183.
58. ACI Committee 374, "Guide for Testing Reinforced Concrete Structural Elements under Slowly Applied Simulated Seismic Loads (ACI 374.2R-13)," American Concrete Institute, Farmington Hills, MI, 2013, 18 pp.
59. Moehle, J., *Seismic Design of Reinforced Concrete Buildings*, McGraw-Hill Education, New York, 2015.
60. Collins, M. P.; Mitchell, D.; Adebar, P.; and Vecchio, F. J., "A General Shear Design Method," *ACI Structural Journal*, V. 93, No. 1, Jan.-Feb. 1996, pp. 36-45.
61. Rafi, M. M.; Nadjai, A.; and Ali, F., "Analytical Modeling of Concrete Beams Reinforced with Carbon FRP Bars," *Journal of Composite Materials*, V. 41, No. 22, 2007, pp. 2675-2690. doi: 10.1177/0021998307078728
62. Wight, J. K., *Reinforced Concrete: Mechanics and Design*, Pearson, Hoboken, NJ, 2015.
63. Nagasaka, T.; Fukuyama, H.; and Tanigaki, M., "Shear Performance of Concrete Beams Reinforced with FRP Stirrups," *Fiber-Reinforced-Plastic Reinforcement for Concrete Structures*, SP-138, American Concrete Institute, Farmington Hills, MI, 1993, pp. 789-811.
64. Hassanein, A.; Mohamed, N.; Farghaly, A. S.; and Benmokrane, B., "Modeling of Hysteretic Response for Concrete Shear Walls Reinforced with Glass Fiber-Reinforced Polymer Bars," *ACI Structural Journal*, V. 116, No. 6, Nov. 2019, pp. 17-29. doi: 10.14359/51716798
65. Mohamed, N.; Farghaly, A. S.; Benmokrane, B.; and Neale, K. W., "Experimental Investigation of Concrete Shear Walls Reinforced with Glass Fiber–Reinforced Bars under Lateral Cyclic Loading," *Journal of Composites for Construction*, ASCE, V. 18, No. 3, 2014, p. A4014001. doi: 10.1061/(ASCE)CC.1943-5614.0000393